CHEMISTRY
A EUROPEAN JOURNAL

DOI: 10.1002/chem.200903256

Nano- and Microstructure Fabrication by Using a Three-Component System

Donghak Jang, Ho Yong Lee, Miae Park, Seong Ryong Nam, and Jong-In Hong*[a]

Abstract: Two-component amphiphiles based on hydrogen-bonded complexes between terephthaloylbisalanine (H_2TBA) and dodecylamine (DA) are able to self-assemble into nano- and microsized superstructures in an aqueous solvent. It is possible to modulate the morphology of these self-assembled superstructures by modifying the composition of the complexes, which can be achieved by changing the molar ratio of the two components or by changing the chirality of H_2TBA. For example, right-handed microhelical ribbon structures were formed with L-TBA$_{1.0}$DA$_{2.0}$, whereas in the case of *rac*-TBA$_{1.0}$DA$_{2.0}$, flat ribbonlike structures were observed. Although L-TBA$_{1.0}$DA$_{1.0}$ exhibited entangled fibrous structures, *rac*-TBA$_{1.0}$DA$_{1.0}$ exhibited wire structures. Different ratios of H_2TBA and DA were self-assembled into fiber-, wire-, and tubulelike superstructures, as well as monoclinic, columnar, and lamellar aggregation patterns. The self-assembled superstructures of TBA$_x$DA$_y$ were significantly changed by adding metal ions. Transition metal (Cd^{II}, Co^{II}, and Zn^{II}) complexes with L-TBA$_x$DA$_y$ self-assembled into rod-, tubule-, wire-, and platelike superstructures. Metal-ion complexes with *rac*-TBA$_x$DA$_y$ exhibited different superstructures. Our work suggests that it is possible to fabricate a wide variety of nano- and microsized superstructures by using two- and three-component amphiphiles.

Keywords: amphiphiles · hydrogels · nanostructures · self-assembly · transition metals

Introduction

Amphiphilic molecules self-assemble into various types of nano- or microstructures, such as micelles, vesicles, fibers, tubules, rods, and helices, in aqueous environments.[1] Amphiphilic molecules derived from peptides,[2] carbohydrates,[3] metal complexes,[4] steroids,[5] and dendrimers[6] have been successfully utilized to fabricate a wide variety of self-assembled structures. Morphological changes in nano- or microstructures depend on solvent polarity and the structural changes and relative fractions of the hydrophilic and hydrophobic groups. These self-assembled superstructures are not only essential parts of biological systems, such as cell membranes, they can also be applied in functional materials for molecular probes, carriers, or optoelectronic devices.[7]

The use of multicomponent amphiphilic systems, as well as single-molecule amphiphilic systems, has also been attempted for nano- or microstructure fabrication.[8] Recently, we reported examples of a two-component gelator system, in which a variety of organogels were produced by the self-assembly of two organogelators, 3,5-bis(dodecanoylamino)-benzoic acid and aromatic amines, in nonaromatic hydrocarbon solvents, through hydrogen bonding, aromatic stacking, and van der Waals interactions.[8d] We found that the shape and size of the aromatic amine has a significant effect on the gel properties, as well as their superstructures. The most important feature of the two-component systems is that the morphology can be easily modulated by changing the molar ratio of the two components or by changing one of the two components. In addition, physical and optoelectronic properties of the self-assembled structures also can be easily modulated by modifying one component.

Incorporating metal ions into organic nanostructures is a good method for generating novel organic nanostructures and expanding their applications. The different coordination geometries of transition metal ions induce different shapes in the coordination complexes, which results in a wide variety of superstructures.[9] Since metal–ligand interactions are known to spontaneously induce cross linking between building blocks, a variety of superstructures can be constructed. In addition, metal-embedded organic superstructures can be used as templates for the fabrication of inorganic nanostruc-

[a] D. Jang, Dr. H. Y. Lee, M. Park, Dr. S. R. Nam, Prof. J.-I. Hong
Department of Chemistry, College of Natural Sciences
Seoul National University, Seoul 151-747 (Republic of Korea)
Fax: (+82) 2-889-1568
E-mail: jihong@snu.ac.kr

Supporting information for this article is available on the WWW under http://dx.doi.org/10.1002/chem.200903256.

tures, and provide the advantage of introducing various new functions.[10] Herein, we report a simple method to control the morphology of organic nano- or microstructures by altering the ratio of the two organic components and incorporating various metal ions into the complexes.

As shown in Scheme 1, the basic building blocks used in this study are composed of terephthaloylbisalanine (H_2TBA), which have symmetric terminal carboxylic acid groups, and dodecylamine (DA).[11] The charged hydrogen-bonded complexes (abbreviated as TBA_xDA_y) between H_2TBA and DA act as amphiphiles in water: the TBA–ammonium complex acts as the hydrophilic head component and the dodecyl group of DA acts as the hydrophobic tail component. Therefore, TBA_xDA_y can self-assemble into various superstructures in an aqueous solvent. L-H_2TBA and *rac*-H_2TBA were prepared to see if chirality would exert any effect on the morphology of the superstructures. Another relevant point is that the carboxylate group in TBA can bind, not only to ammonium ions, but also to metal ions. The incorporation of metal ions is accompanied by structural changes in the supramolecular structure formed by the aggregation of the basic building blocks, resulting in new nano- or microstructures. Moreover, the resulting supramolecular structures can be easily tuned by changing the ratio of DA to H_2TBA, the chirality of H_2TBA, and by incorporating metal ions.

Results and Discussion

Mixing ratio and gel properties: The gelation behavior of the complexes of TBA_xDA_y was tested in deionized water. Solutions of H_2TBA and DA in MeOH in various ratios were concentrated and the resulting white solids were suspended in deionized water and heated to give rise to a colorless solution, which was then cooled to room temperature. Upon standing at room temperature, the clear solution turned into an opaque solution or gel. The mixing ratio and gel properties are listed in Table 1. The 1:2 mixture of L- or *rac*-H_2TBA and DA ($TBA_{1.0}DA_{2.0}$) became an opaque gel within 10 min. In the case of the 1:1 mixture of L- or *rac*-H_2TBA and DA ($TBA_{1.0}DA_{1.0}$), precipitates were formed after 20 min. Although *rac*-$TBA_{1.0}DA_{1.5}$ turned into an opaque gel after 1 h, L-$TBA_{1.0}DA_{1.5}$ remained in solution. Both $TBA_{1.5}DA_{1.0}$ and $TBA_{2.0}DA_{1.0}$ became opaque gels within one day.

Table 1. Mixing ratio and gel properties of two- and three-component systems.[a]

Composition	Morphology	Composition	Morphology
L-$TBA_{1.0}DA_{2.0}$	G	*rac*-$TBA_{1.0}DA_{2.0}$	G
L-$TBA_{1.0}DA_{1.5}$	S	*rac*-$TBA_{1.0}DA_{1.5}$	G
L-$TBA_{1.0}DA_{1.0}$	P	*rac*-$TBA_{1.0}DA_{1.0}$	P
L-$TBA_{1.5}DA_{1.0}$	G	*rac*-$TBA_{1.5}DA_{1.0}$	G
L-$TBA_{2.0}DA_{1.0}$	G	*rac*-$TBA_{2.0}DA_{1.0}$	G
L-$TBA_{1.0}DA_{1.0}Zn^{II}$	G	*rac*-$TBA_{1.0}DA_{1.0}Zn^{II}$	NS
L-$TBA_{1.0}DA_{1.0}Cd^{II}$	G	*rac*-$TBA_{1.0}DA_{1.0}Cd^{II}$	G
L-$TBA_{1.0}DA_{1.0}Co^{II}$	G	*rac*-$TBA_{1.0}DA_{1.0}Co^{II}$	G
L-$TBA_{1.0}DA_{1.5}Zn^{II}$	P	*rac*-$TBA_{1.0}DA_{1.5}Zn^{II}$	NS
L-$TBA_{1.0}DA_{1.5}Cd^{II}$	P	*rac*-$TBA_{1.0}DA_{1.5}Cd^{II}$	G
L-$TBA_{1.0}DA_{1.5}Co^{II}$	P	*rac*-$TBA_{1.0}DA_{1.5}Co^{II}$	G

[a] G = gel, S = clear solution, P = precipitate, and NS = not soluble.

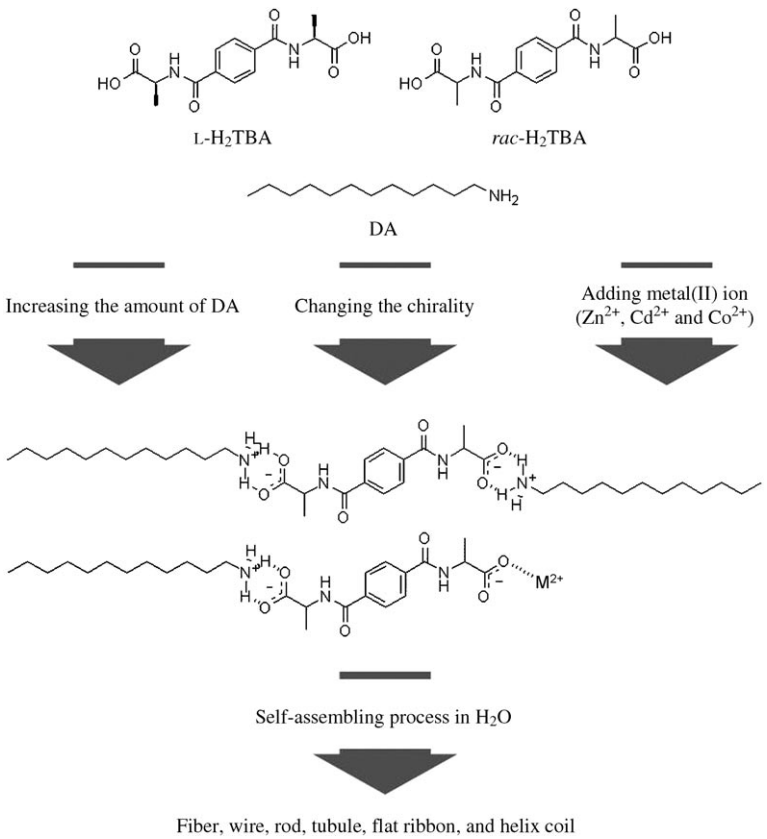

Scheme 1. The chemical structures of L-H_2TBA, *rac*-H_2TBA, and DA, and a schematic representation of the fabrication of various self-assembled structures by using two- and three-component amphiphiles.

Incorporation of metal ions into TBA_xDA_y was accomplished by suspending the white solid from the H_2TBA–DA mixtures in deionized water containing metal ions (1 equiv). The suspension was heated until clear, followed by cooling to room temperature. The mixing ratio and gel properties are listed in Table 1. Upon incubation at room temperature, Cd^{II} and Co^{II} complexes of *rac*-$TBA_{1.0}DA_{1.0}$ and *rac*-$TBA_{1.0}DA_{1.5}$ turned into opaque gels within 3 min, but

the corresponding Zn^{II} complexes were not soluble in water, even after heating. In the cases of the Zn^{II}, Cd^{II}, and Co^{II} complexes of L-$TBA_{1.0}DA_{1.0}$, opaque gels were formed within one day. In contrast, Zn^{II}, Cd^{II}, and Co^{II} complexes of L-$TBA_{1.0}DA_{1.5}$ immediately formed insoluble solids upon heating.

Morphologies of TBA_xDA_y aggregates: To confirm the self-assembled superstructures of TBA_xDA_y, SEM and energy-filtering transmission electron microscopy (EF-TEM) images were obtained. According to the EM images, the self-assembled superstructures of $TBA_{1.0}DA_{2.0}$ were significantly changed by the chirality of H_2TBA. Right-handed microhelical-ribbon structures were formed in L-$TBA_{1.0}DA_{2.0}$, in which the helical pitch was 2–3 μm (Figure 1a). However,

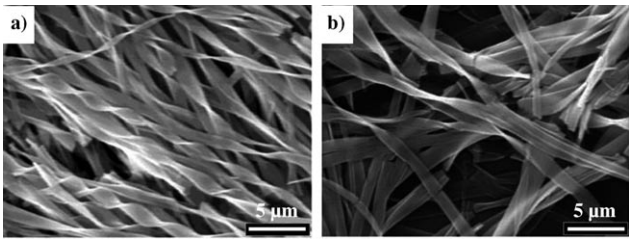

Figure 1. SEM images of a) L-$TBA_{1.0}DA_{2.0}$ and b) *rac*-$TBA_{1.0}DA_{2.0}$.

in the case of *rac*-$TBA_{1.0}DA_{2.0}$, flat ribbonlike structures were observed (Figure 1b). In the case of helicity-inducing ligands, racemic ligands usually induced an equal amount of right- and left-handed helical structures.[12] However, our results are well matched with those of the groups of Fuhrhop and Oda, in which the resulting superstructure lost helicity, when racemic ligands instead of chiral ligands were used.[8b,c]

Changing the mixing ratio also dramatically changed the superstructures of the TBA_xDA_y assemblies. Nanotubules with a diameter of approximately 500 nm were observed in *rac*-$TBA_{1.0}DA_{1.5}$. SEM images revealed a hollow, rectangular shape at the edge (Figure 2a, b). We were able to capture the hollow shape of *rac*-$TBA_{1.0}DA_{1.5}$ with EF-TEM (Figure S1 in the Supporting Information). Although L-$TBA_{1.0}DA_{1.0}$ showed entangled fibrous structures, *rac*-$TBA_{1.0}DA_{1.0}$ showed wire structures (Figure 2c, d). TBA-enriched TBA_xDA_y, such as $TBA_{1.5}DA_{1.0}$ and $TBA_{2.0}DA_{1.0}$, self-assembled into wirelike superstructures (Figure S2 in the Supporting Information).

Morphologies of $TBA_xDA_yM^{II}$ aggregates: As expected, self-assembled superstructures of TBA_xDA_y were significantly changed by the addition of metal ions. As shown in Figure 3, SEM and EF-TEM images of Cd^{II} complexes of L-$TBA_{1.0}DA_{1.0}$ showed structural changes from fibrous to rodlike structures with diameters of about 100 nm (Figure 3a). Surprisingly, tubule-shaped superstructures were obtained by adding Co^{II} ions to L-$TBA_{1.0}DA_{1.0}$ (Figure 3b). The tubules had external and internal diameters of approximate-

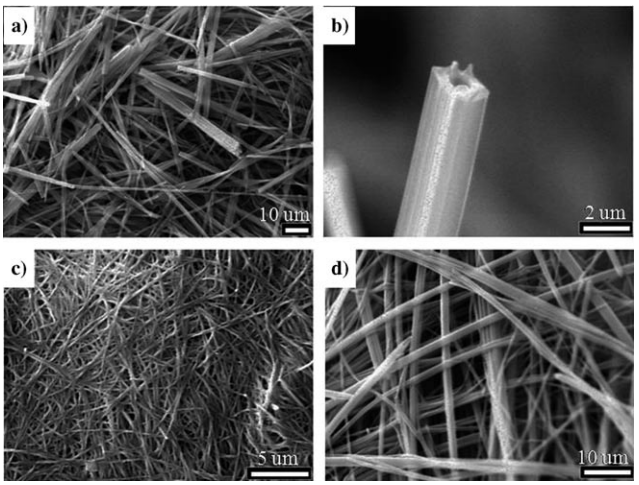

Figure 2. SEM images of a) *rac*-$TBA_{1.0}DA_{1.5}$, b) the hollow shape of the edge of *rac*-$TBA_{1.0}DA_{1.5}$, c) L-$TBA_{1.0}DA_{1.0}$, and d) *rac*-$TBA_{1.0}DA_{1.0}$.

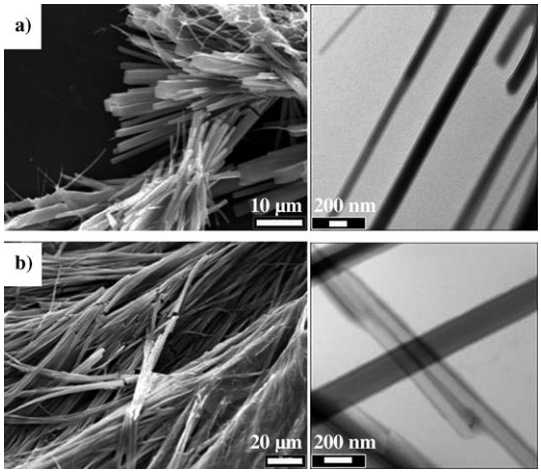

Figure 3. SEM (left) and EF-TEM (right) images of a) L-$TBA_{1.0}DA_{1.0}Cd^{II}$ and b) L-$TBA_{1.0}DA_{1.0}Co^{II}$.

ly 150 and 100 nm, respectively. However, the superstructures of L-$TBA_{1.0}DA_{1.0}$ did not show any significant change after adding Zn^{II} ions (Figure S3 in the Supporting Information).

Interestingly, although L-$TBA_{1.0}DA_{1.5}$ remained in solution, metal complexes with L-$TBA_{1.0}DA_{1.5}$ formed precipitates. According to the SEM and EF-TEM images, the precipitates were a bundle of highly ordered superstructures. As shown in Figure 4a and b, L-$TBA_{1.0}DA_{1.5}Zn^{II}$ and L-$TBA_{1.0}DA_{1.5}Cd^{II}$ self-assembled into nanosized wire structures, with diameters of about 140 and 100 nm, respectively. However, a Co^{II} complex with L-$TBA_{1.0}DA_{1.5}$ self-assembled into tubule structures with external and internal diameters of about 160 and 50 nm, respectively (Figure 4c, d).

On the other hand, metal ion complexes with *rac*-TBA_xDA_y exhibited different superstructures. SEM images revealed that the Cd^{II} complexes with *rac*-$TBA_{1.0}DA_{1.0}$ and *rac*-$TBA_{1.0}DA_{1.5}$ had platelike super-

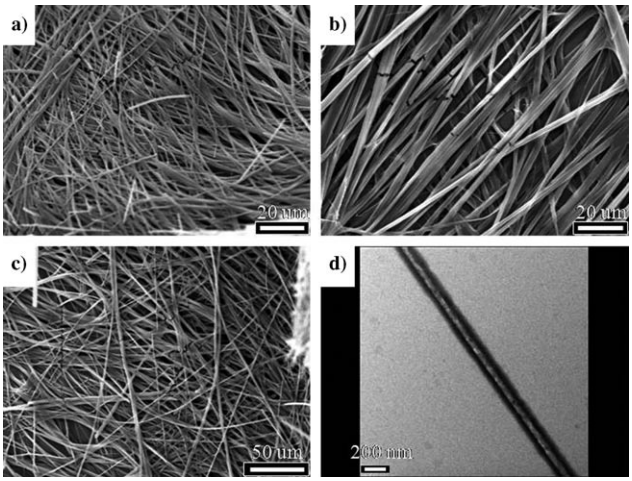

Figure 4. SEM images of a) L-$TBA_{1.0}DA_{1.5}Zn^{II}$, b) L-$TBA_{1.0}DA_{1.5}Cd^{II}$, and c) L-$TBA_{1.0}DA_{1.5}Co^{II}$. d) EF-TEM image of L-$TBA_{1.0}DA_{1.5}Co^{II}$ shows a hollow shape.

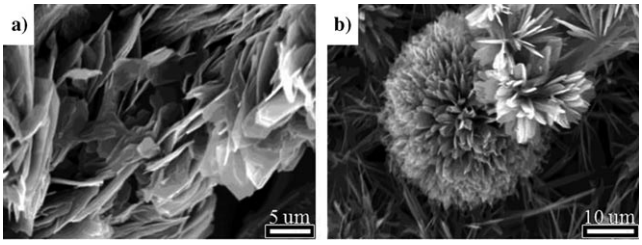

Figure 5. SEM images of Cd^{II} complexes with a) *rac*-$TBA_{1.0}DA_{1.0}Cd^{II}$ and b) *rac*-$TBA_{1.0}DA_{1.5}Cd^{II}$.

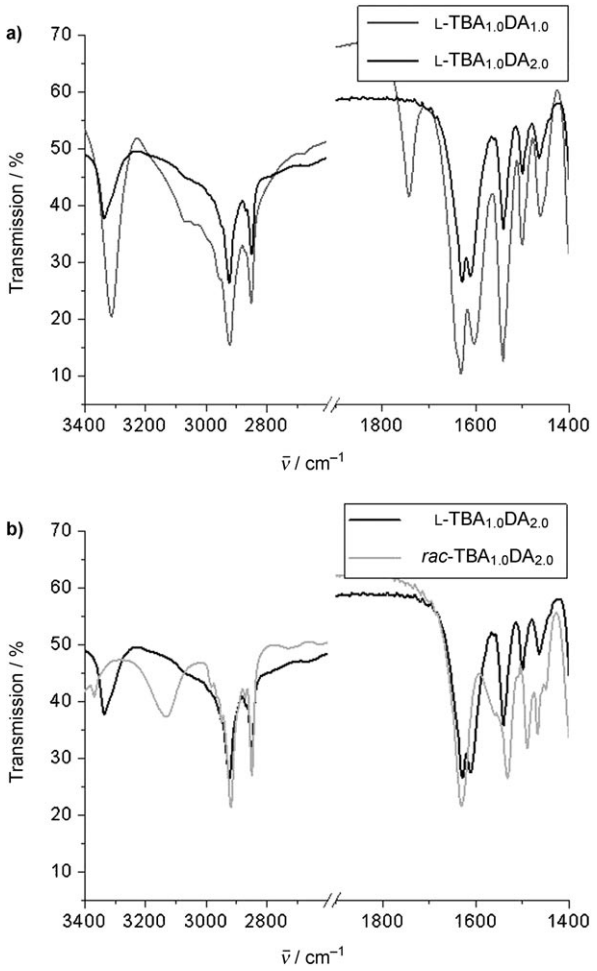

Figure 6. a) FTIR spectra of L-$TBA_{1.0}DA_{1.0}$ and L-$TBA_{1.0}DA_{2.0}$. b) FTIR spectra of L-$TBA_{1.0}DA_{2.0}$ and *rac*-$TBA_{1.0}DA_{2.0}$.

structures (Figure 5), whereas *rac*-$TBA_{1.0}DA_{1.0}$ and *rac*-$TBA_{1.0}DA_{1.5}$ showed wire and tubule structures, respectively (Figure 2). Zn^{II} and Co^{II} complexes with *rac*-$TBA_{1.0}DA_{1.0}$ and *rac*-$TBA_{1.0}DA_{1.5}$ did not form ordered superstructures.

FTIR spectroscopic analysis: FTIR spectroscopic analysis was employed to provide a better insight into the self-assembled structures of the xerogels and the dried precipitates of the TBA_xDA_y aggregates. The FTIR spectra of L- and *rac*-$TBA_{1.0}DA_{2.0}$ only showed two absorptions at 1611 and 1395 cm^{-1} corresponding to the typical asymmetrical and symmetrical stretching vibrations of the carboxylate, but did not show absorptions of the carboxylic acid (Figure 6a). These absorption spectra indicate that all carboxylic acids in L- and *rac*-$TBA_{1.0}DA_{2.0}$ are fully deprotonated during the self-assembling process. However, the absorption spectrum of L- and *rac*-$TBA_{1.0}DA_{1.0}$ showed three absorptions at 1743, 1603, and 1399 cm^{-1}. The absorption at 1743 cm^{-1} corresponds to the carboxylic acid stretching vibration and the absorptions at 1603 and 1399 cm^{-1} correspond to the carboxylate stretching vibrations. Therefore, the absorption spectrum of L-$TBA_{1.0}DA_{1.0}$ indicates that both carboxylic acid and carboxylate ion moieties coexist in the complex during the self-assembling process. All complexes have absorptions corresponding to CH_2 asymmetrical and symmetrical stretching vibrations at 2918–2923 and 2850–2851 cm^{-1}, respectively. These CH_2 stretching absorptions signify that part of the hydrocarbon chains of DA have a *gauche* conformation in the self-assembled structures, which indicates that the hydrocarbon chains are arrayed in a disordered state.[13]

There was no significant change in the carbonyl absorption bands of the carboxylic acids upon changing the chirality of H_2TBA. However, the absorption bands of the amide N–H stretching vibration and amide I in L-TBA_xDA_y showed a slight shift to a lower wavenumber than *rac*-TBA_xDA_y, which means that L-TBA_xDA_y forms stronger intermolecular hydrogen-bonding networks than *rac*-TBA_xDA_y (Figure 6b). The CH_2 asymmetrical and symmetrical stretching vibrations of *rac*-$TBA_{1.0}DA_{1.0}$ are almost the same as those of L-$TBA_{1.0}DA_{1.0}$. On the other hand, the CH_2 asymmetrical and symmetrical stretching vibrations of *rac*-$TBA_{1.0}DA_{2.0}$ shifted to lower wavenumbers, (2918 and 2850 cm^{-1}), than L-$TBA_{1.0}DA_{2.0}$. This indicates that the hydrocarbon chains in the self-assembled structure of ;*rac*-$TBA_{1.0}DA_{2.0}$ aggregates have a more crystalline conformation than the L-complex.

Powder XRD analysis: We performed powder XRD analyses on the dried samples of L-TBA_xDA_y, *rac*-TBA_xDA_y, and L-$TBA_{1.0}DA_{1.0}M^{II}$ to obtain more information on the aggregation patterns in the two- and three-component systems. The diffraction pattern of $TBA_{1.0}DA_{1.0}$ showed three similar intense peaks in the small-angle region, irrespective of the chirality (Figure S6a, b in the Supporting Information). These diffraction patterns indicate that both L- and *rac*-$TBA_{1.0}DA_{1.0}$ self-assembled into superstructures with monoclinic unit cell structures and that changing the chirality has little influence on the unit cell parameters (Table 2). These results were also supported by the fact that L- and *rac*-$TBA_{1.0}DA_{1.0}$ have the same fibrous superstructure. However, $TBA_{1.0}DA_{2.0}$ showed distinct changes, not only in the diffraction pattern (Figure S6c, d in the Supporting Information), but also in EM images (Figure 1). Unlike $TBA_{1.0}DA_{1.0}$, ribbonlike superstructures of L- and *rac*-$TBA_{1.0}DA_{2.0}$ aggregates had different unit cell structures. When *rac*-H_2TBA was replaced with L-H_2TBA, the unit cell structure of the $TBA_{1.0}DA_{2.0}$ aggregates changed from lamellar to columnar (Table 2). Close packing aggregation of L-$TBA_{1.0}DA_{2.0}$ due to stronger intermolecular hydrogen-bonding interactions promoted a one-directional self-assembling process. As a result, L-$TBA_{1.0}DA_{2.0}$ was able to self-assemble into a helical ribbon structure (Figure 1a). Interestingly, the diffraction pattern of *rac*-$TBA_{1.0}DA_{1.5}$ aggregates showed peaks from *rac*-$TBA_{1.0}DA_{1.0}$ and *rac*-$TBA_{1.0}DA_{2.0}$ (Figure 7). The mixed diffraction pattern revealed that both the monoclinic unit cell structure from *rac*-$TBA_{1.0}DA_{1.0}$ and the lamellar unit cell structure from *rac*-$TBA_{1.0}DA_{2.0}$ coexisted in one self-assembled structure. However, the two unit cell structures did not develop individually into original self-assembled structures, but participated in the self-assembly process to make one superstructure.

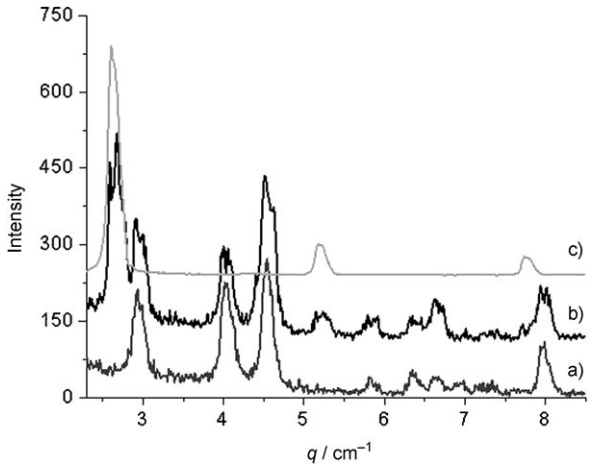

Figure 7. Overlapped X-ray diffraction patterns of a) *rac*-$TBA_{1.0}DA_{1.0}$, b) *rac*-$TBA_{1.0}DA_{1.5}$, and c) *rac*-$TBA_{1.0}DA_{2.0}$.

Table 2. Unit cell structures and parameters of TBA_xDA_y and $TBA_xDA_yM^{II}$.

Composition	a [Å]	b [Å]	c [Å]	α [°]	β [°]	γ [°]	Unit cell structure
L-$TBA_{1.0}DA_{1.0}$	16.21	14.11	24.86	90.00	60.50	90.00	monoclinic
L-$TBA_{1.0}DA_{2.0}$	14.50	14.50				97.20	columnar
rac-$TBA_{1.0}DA_{1.0}$	15.90	13.84	24.62	90.0	60.50	90.00	monoclinic
rac-$TBA_{1.0}DA_{2.0}$	24.12						lamellar
L-$TBA_{1.0}DA_{1.0}Zn^{II}$	33.50	21.22	27.87	90.00	49.60	90.00	monoclinic
L-$TBA_{1.0}DA_{1.0}Cd^{II}$	32.91	25.96	26.39	90.00	52.10	90.00	monoclinic
L-$TBA_{1.0}DA_{1.0}Co^{II}$	30.12	26.59	28.40	90.00	62.00	90.00	monoclinic

To study the influence of metal ions on the self-assembled structures in the three-component system, X-ray diffraction patterns of Zn^{II}, Cd^{II}, and Co^{II} complexes with L-$TBA_{1.0}DA_{1.0}$ were compared with their nonmetal complexes. All of the L-$TBA_{1.0}DA_{1.0}M^{II}$ aggregates had monoclinic unit cell structures like their nonmetal complexes. However, L-$TBA_{1.0}DA_{1.0}M^{II}$ aggregates had different unit cell parameters. The β value of the unit cell showed a gradual increase upon the respective addition of Zn^{II}, Cd^{II}, and Co^{II} to L-$TBA_{1.0}DA_{1.0}$ (Table 2). The metal–TBA interaction did not influence the interaction between TBA and DA, which was reflected in the same unit cell structures of both $TBA_{1.0}DA_{1.0}$ and $TBA_{1.0}DA_{1.0}M^{II}$. However, the different coordination geometry of metal ions should give rise to changes in unit cell parameters, which would cause different self-assembled superstructures.[14] Shimizu et al. also mentioned that the coordination geometry of metal ions induced morphological changes in self-assembled structures.[10b]

Conclusion

We have suggested a simple way to fabricate nano- or microsized superstructures by using noncovalent interactions. Various superstructures were constructed by the self-assembly of a simple amino acid derivative and aliphatic amine. The incorporation of metal ions into the mixtures of H_2TBA–DA resulted in a variety of new self-assembled superstructures, such as nano- and microstructures. The diversity of superstructures resulting from the addition of metal ions might be due to the different coordination numbers, geometry, and binding affinities of the metal ions. These differences can induce dramatic changes in the basic building blocks themselves and, eventually, in the aggregation mode. This method can be applied to the fabrication of various conducting nanomaterials or to organic templates for inorganic nanostructures.

Experimental Section

Materials and synthesis: All chemicals and solvents were purchased from Aldrich or Tokyo Kasei Chemicals, and used without further purification.

^{1}H and ^{13}C NMR spectra were measured on a Bruker Advance 300 spectrometer. The XWINNMR program was used for the pulse program. The GC–MS was obtained with a JEOL JMS-AX505WA or HP 5890 Series II instrument, by using the FAB method.

Preparation of samples: H_2TBA and DA were mixed in MeOH in various ratios. The suspensions were heated or sonicated until they turned into a clear solution. Then, the solution in MeOH was evaporated in vacuo until white solids were generated. Two-component amphiphilic complexes were prepared by suspending the resulting white solids (TBA_xDA_y; 10 mg) in deionized water (500 μL). The suspension was heated until clear, followed by cooling, and incubating at RT until it turned into either a gel or an insoluble solid. Three-component amphiphilic complexes were prepared by suspending TBA_xDA_y (10 mg) in deionized water (500 μL) containing $M(NO_3)_2{\cdot}xH_2O$ (1 equiv, M = Zn, Cd, Co, Cu). The suspension was heated until clear, followed by cooling, and incubating at RT until it turned into either a gel or an insoluble solid.

Electron microscopy images: For SEM imaging of the two- or three-component systems, the gels or precipitates were diluted with deionized water (500 μL). The diluted suspensions were dropped onto a slide glass, and then air dried. The prepared specimens were coated with Au. For TEM imaging of the two- or three-component systems, gels or precipitates were diluted with deionized water (4.5 mL). The diluted suspensions were dropped onto a carbon grid, and then air dried. TEM images were obtained without staining. SEM images were observed with a JEOL-JSM 5410 LV instrument. EF-TEM images were observed with a Carl Zeiss-LIBRA 120.

FTIR spectra measurement: To obtain FTIR spectra, the gels or precipitates were dried at RT. The dried samples and KBr were mixed and ground to form a fine powder. By using the powder, a KBr and gel-containing pellet was prepared. FTIR spectra were obtained with a JASCO FT/IR-660 Plus.

Powder X-ray diffraction analysis: To obtain X-ray diffraction patterns, the gels or precipitates were dried at RT. The dried samples were analyzed with a Bruker D5005 diffractometer. The diffraction radius was $2\theta = 3$–$13°$, the step size was 0.02, and the scan speed was $1° \text{min}^{-1}$. The wavelength of the X-ray was 1.5406 Å (the generator was 40 kV and 40 mA).

Preparation of terephthaloylbisalanine methyl ester (L- and *rac*-MeTBA): Terephthaloyl chloride (2.37 g, 11.7 mmol) and L-(or *rac*-)alanine methyl ester hydrochloride (3.06 g, 21.9 mmol) were suspended in CH_2Cl_2 (150 mL) under an N_2 atmosphere at 0 °C. Triethylamine (6 mL, 43.0 mmol) was carefully added to the mixture, and then stirred for 3 h at RT. The reaction mixture was washed three times with H_2O. The organic residues were dried over Na_2SO_4 and evaporated to give a pale yellow solid. The crude product was purified by recrystallization with CH_2Cl_2 and hexane to give rise to a white solid (1.077 g, 29 %). L-MeTBA: ^{1}H NMR (300 MHz, $CDCl_3$): $\delta = 1.57$ (d, $^3J(H,H) = 7.14$ Hz, 6H; CH_3), 3.83 (s, 6H; CH_3), 4.83 (m, 2H; CH), 6.79 (d, $^3J(H,H) = 6.64$ Hz, 2H; NH), 7.90 ppm (s, 4H; CH); *rac*-MeTBA: ^{1}H NMR (300 MHz, $CDCl_3$): $\delta = 1.57$ (d, $^3J(H,H) = 7.14$ Hz, 6H; CH_3), 3.83 (s, 6H; CH_3), 4.83 (m, 2H; CH), 6.79 (d, $^3J(H,H) = 6.64$ Hz, 2H; NH), 7.90 ppm (s, 4H; CH).

Preparation of terephthaloylbisalanine (L- and *rac*-H_2TBA): A 1 N aqueous solution of NaOH (30 mL) was added to a solution of MeTBA (1.077 g, 3.20 mmol) in EtOH (10 mL) and then stirred for 3 h at RT. After which time, the EtOH was evaporated and the aqueous residue was acidified with 1 N aqueous HCl to pH 1. H_2TBA was purified by recrystallization in acidic aqueous conditions to give rise to a white solid. L-H_2TBA: ^{1}H NMR (300 MHz, [D_6]DMSO): $\delta = 1.41$ (d, $^3J(H,H) = 7.35$ Hz, 6H; CH_3), 4.44 (m, 2H; CH), 7.97 (s, 4H; CH), 8.80 (d, $^3J(H,H) = 7.17$ Hz, 2H; NH), 12.72 ppm (brs, 2H; OH); ^{13}C NMR (75 MHz, [D_6]DMSO): $\delta = 17.338$, 48.697, 127.828, 136.723, 165.908, 174.541 ppm; HRMS (FAB$^+$): *m/z* calcd for $C_{14}H_{17}N_2O_6$: 309.1087; found: 309.1086; *rac*-H_2TBA: ^{1}H NMR (300 MHz, [D_6]DMSO): $\delta = 1.41$ (d, $^3J(H,H) = 7.35$ Hz, 6H; CH_3), 4.44 (m, 2H; CH), 7.97 (s, 4H; CH), 8.80 (d, $^3J(H,H) = 7.17$ Hz, 2H; NH), 12.72 ppm (brs, 2H; OH); ^{13}C NMR (75 MHz, [D_6]DMSO): $\delta = 17.338$, 48.697, 127.828, 136.723, 165.908, 174.541 ppm; HRMS (FAB$^+$): *m/z* calcd for $C_{14}H_{17}N_2O_6$: 309.1087; found: 309.1086.

Acknowledgements

We thank the KRF (grant no.: 2008-314-1-C00206) for financial support. M.P. is the recipient of the BK 21 fellowship. We thank Professor M. Lee for advice.

[1] For comprehensive reviews, see: a) J.-H. Ryu, D.-J. Hong, M. Lee, *Chem. Commun.* **2008**, 1043–1054; b) T. Shimizu, M. Masuda, H. Minamikawa, *Chem. Rev.* **2005**, *105*, 1401–1443; c) F. J. M. Hoeben, P. Jonkheijm, E. W. Meijer, A. P. H. J. Schening, *Chem. Rev.* **2005**, *105*, 1491–1546; d) R. V. Ulijn, A. M. Smith, *Chem. Soc. Rev.* **2008**, *37*, 664–675; e) X. Zhao, S. Zhang, *Chem. Soc. Rev.* **2006**, *35*, 1105–1110.

[2] a) J. D. Hartgerink, E. Beniash, S. I. Stupp, *Science* **2001**, *294*, 1684–1688; b) Y. B. Lim, E. Lee, M. Lee, *Angew. Chem.* **2007**, *119*, 9169–9172; *Angew. Chem. Int. Ed.* **2007**, *46*, 9011–9014.

[3] a) J. H. Jung, G. John, K. Yoshida, T. Shimizu, *J. Am. Chem. Soc.* **2002**, *124*, 10674–10675; b) S. Bhattacharya, S. N. G. Acharya, *Chem. Mater.* **1999**, *11*, 3504–3511.

[4] a) J. Zhang, Y.-F. Song, L. Cronin, T. Liu, *J. Am. Chem. Soc.* **2008**, *130*, 14408–14409; b) M. Shirakawa, N. Fujita, T. Tani, K. Kaneko, M. Ojima, A. Fujii, M. Ozaki, S. Shinkai, *Chem. Eur. J.* **2007**, *13*, 4155–4162.

[5] a) C. Geiger, M. Stanesau, L. Chen, D. G. Whitten, *Langmuir* **1999**, *15*, 2241–2245; b) N. M. Sangeetha, U. Maitra, *Chem. Soc. Rev.* **2005**, *34*, 821–836; c) Y. C. Lin, B. Kachar, R. G. Weiss, *J. Am. Chem. Soc.* **1989**, *111*, 5542–5551.

[6] a) W. D. Jang, D. L. Jiang, T. Aida, *J. Am. Chem. Soc.* **2000**, *122*, 3232–3233; b) F. Gröhn, K. Klein, S. Brand, *Chem. Eur. J.* **2008**, *14*, 6866–6869.

[7] a) H.-J. Kim, J. Lee, T.-H. Kim, T. S. Lee, J. Kim, *Adv. Mater.* **2008**, *20*, 1117–1121; b) J.-K. Kim, E. Lee, Y.-B. Lim, M. Lee, *Angew. Chem.* **2008**, *120*, 4740–4744; *Angew. Chem. Int. Ed.* **2008**, *47*, 4662–4666; c) Y. Che, A. Datar, K. Balakrishnan, L. Zhang, *J. Am. Chem. Soc.* **2007**, *129*, 7234–7235; d) J. P. Hill, W. Jin, A. Kosaka, T. Fukushima, H. Ichihara, T. Shimomura, K. Ito, T. Hashizume, N. Ishii, T. Aida, *Science* **2004**, *304*, 1481–1483; e) S. R. Diegelmann, J. M. Gorham, J. D. Tovar, *J. Am. Chem. Soc.* **2008**, *130*, 13840–13841.

[8] a) K. Hanabusa, T. Miki, Y. Taguchi, T. Koyama, H. Shirai, *J. Chem. Soc. Chem. Commun.* **1993**, 1382–1384; b) J. H. Fuhrhop, P. Schnieder, J. Rosenberg, E. Boekema, *J. Am. Chem. Soc.* **1987**, *109*, 3387–3390; c) R. Oda, I. Huc, S. J. Candau, *Angew. Chem.* **1998**, *110*, 2835–2838; *Angew. Chem. Int. Ed.* **1998**, *37*, 2689–2691; d) H. Y. Lee, S. R. Nam, J.-I. Hong, *J. Am. Chem. Soc.* **2007**, *129*, 1040–1041; e) H. Basit, A. Pal, S. Sen, S. Bhattacharya, *Chem. Eur. J.* **2008**, *14*, 6534–6545; f) .T. Zemb, M. Dubois, B. Deme, T. Gulik-Krzywicki, *Science* **1999**, *283*, 816–819.

[9] a) M. Oh, C. A. Mirkin, *Nature* **2005**, *438*, 651–654; b) H. Maeda, M. Hasegawa, T. Hashimoto, T. Kakimoto, S. Nishio, T. Nakanishi, *J. Am. Chem. Soc.* **2006**, *128*, 10024–10025; c) A. Richard, V. Marchi-Artzner, M.-N. Lalloz, M.-J. Brienne, F. Artzner, T. Gulik-Krzywicki, M.-A. Guedeau-Boudeville, J.-M. Lehn, *Proc. Natl. Acad. Sci. USA* **2004**, *101*, 15279–15284; d) R. J. Mart, K. P. Liem, X. Wang, S. J. Webb, *J. Am. Chem. Soc.* **2006**, *128*, 14462–14463.

[10] a) X.-F. Shen, X.-P. Yan, *Angew. Chem.* **2007**, *119*, 7803–7807; *Angew. Chem. Int. Ed.* **2007**, *46*, 7659–7663; b) M. Kogiso, Y. Zhou, T. Shimizu, *Adv. Mater.* **2007**, *19*, 242–246; c) Y. Zhou, M. Kogiso, C. He, Y. Shimizu, N. Koshizaki, T. Shimizu, *Adv. Mater.* **2007**, *19*, 1055–1058.

[11] See the Experimental Section for the details of preparation and characterization.

[12] a) T. Gulik-Krzywicki, C. Fouquey, J.-M. Lehn, *Proc. Natl. Acad. Sci. USA* **1993**, *90*, 163–167; b) M. S. Spector, J. V. Selinger, A. Singh, J. M. Rodriguez, R. R. Price, J. M. Schnur, *Langmuir* **1998**, *14*, 3493–3500; c) B. N. Thomas, C. M. Lindemann, R. C. Corcoran, C. L. Cotant, J. E. Kirsch, P. J. Persichini, *J. Am. Chem. Soc.* **2002**, *124*, 1227–1233; d) H.-J. Kim, D. Moon, M. S. Lah, J.-I. Hong,

Angew. Chem. **2002**, *114*, 3306–3309; *Angew. Chem. Int. Ed.* **2002**, *41*, 3174–3177.
[13] A. Brizard, C. Aimé, T. Labrot, I. Huc, D. Berthier, F. Artzner, B. Debat, R. Oda, *J. Am. Chem. Soc.* **2007**, *129*, 3754–3762.
[14] H. Y. Lee, J. Park, M. S. Lah, J.-I. Hong, *Cryst. Growth Des.* **2008**, *8*, 587–591.

Received: November 28, 2009
Published online: March 22, 2010

